RSC Advances

PAPER

View Article Online
View Journal | View Issue

Cite this: *RSC Adv.*, 2019, **9**, 5804

Facile synthesis of urchin-like Cs_xWO_3 particles with improved transparent thermal insulation using bacterial cellulose as a template

Chuan-Yan Fan, Jing-Xiao Liu, * Fei Shi,* Shuai Ran, Bin Chen, Jing Zhou, Su-Hua Liu, Xin Song and Jiahong Kang

Urchin-like Cs_xWO_3 particles were synthesized using bacterial cellulose (BC) as a template by the hydrothermal method. The effects of the BC addition amount on the morphology, W^{5+} content and transparent thermal insulation of Cs_xWO_3 were studied. It has been confirmed that abnormal growth of Cs_xWO_3 rods was greatly reduced after introduction of BC into the precursor solution. Moreover, introduction of BC into the precursor solution could significantly improve the transparent thermal insulation properties of the Cs_xWO_3 film. In particular, when the BC amount was appropriate, the prepared Cs_xWO_3 film exhibited better visible transparency, with the visible light transmittance (T_{Vis}) more than 60%. In addition, the urchin-like particles could be transformed into small size nanorods after H_2 heat-treatment, exhibiting excellent visible light transparency and thermal insulation performance. In particular, it has been proved that the 20BC-HT-Cs_xWO_3 film exhibits excellent thermal insulation performance, and shows broad application prospects in the field of solar heat filters and energy-saving window glass.

Received 13th September 2018
Accepted 4th February 2019

DOI: 10.1039/c8ra07626j

rsc.li/rsc-advances

1. Introduction

As is well known, near infrared (780–2500 nm) energy accounts for about 50% of the solar radiation spectrum, and ordinary window glass hardly has near infrared shielding ability.[1] In general, coating or sticking a transparent heat-insulation film[2,3] on the glass surface is an effective way to achieve energy-saving building window glass. At present, there have been many reports about inorganic functional particles used for preparing transparent heat-insulating films such as indium tin oxide (ITO),[4,5] antimony doped tin oxide (ATO),[6] VO_2 (ref. 7) and $W_{3-x}O_3$ (ref. 8) *etc.* However, in recent years, hexagonal M_xWO_3 (M = Na,[9] K,[10–12] Rb,[13] Cs,[14–18] NH_4 (ref. 19–21) *etc.*) particles have been attracting considerable interest due to their more excellent near infrared absorption/shielding ability and transparent thermal insulation. In particular, the hexagonal Cs_xWO_3 particles exhibit outstanding transparent thermal insulation and energy-saving performance, and also have potential application prospects in the field of photothermal treatment of cancer[22–25] and photocatalysis.[26,27]

As is reported, the transparent thermal insulation performance of M_xWO_3 can be further improved by increasing the relative content of W^{5+} in the particles[1,28] or by doping some cations or anions such as Pt^{X+1}, Mo^{X+} (ref. 29) and F^- (ref. 30) *etc.* Nevertheless, the particle size control of M_xWO_3 is also a very important factor for realizing its practical applications.[31] It is suggested that particles with sizes well below the wavelength of visible light can effectively depress visible light scattering and achieve a clear vision.[32] Moreover, decreasing the size of the particles can make the near-infrared cut-off shift to the visible light,[33] and thus can effectively improve the near-infrared shielding ability. In addition, from the view of film processing, tiny particles are relatively easy to disperse into the solvent or solid matrix and is favorable for obtaining uniform thermal insulation films.

In practice, small size Cs_xWO_3 particles can be synthesized by solvothermal method using ethanol, tungsten hexachloride and cesium hydroxide as raw materials.[28,34] However, unfortunately, solvothermal method is not suitable for large-scale industrial production, because the raw materials such as tungsten hexachloride are expensive and the solvothermal synthesis process has an increased risk of environmental pollution owing to the utility of tungsten hexachloride and organic solvents. Generally, hydrothermal synthesis of M_xWO_3 from sodium tungstate using water as solvent is more desirable for realizing its commercial application. However, it is often difficult to synthesize M_xWO_3 particles with high uniformity and small size by hydrothermal method owing to the large amount of water in the precursor solution. It has been confirmed that trace amount of water in the solvent play an important role in the growth of M_xWO_3 nanorods.[28] But

Key Laboratory of New Materials and Modification of Liaoning Province, School of Textile and Materials Engineering, Dalian Polytechnic University, Dalian 116034, PR China. E-mail: jxliu2366@163.com; shifei@dlpu.edu.cn; Fax: +86 411 86323438; Tel: +86 411 86323708

according to our previous research results, too much amount of water would have great negative effects on controlling the growth of crystalline grain during solvothermal process. Therefore, there is an urgent need to develop a innovative way of preparing M_xWO_3 particles with small grain size and better transparent thermal insulation by a hydrothermal method with low-cost and low-pollution to environment.

Bacterial cellulose (BC), as a natural biopolymer, has received growing interest lately due to its remarkable physico-chemical properties such as high crystallinity, high water holding capacity and high tensile strength *etc.* BC can also act as a template in the synthesis of functional nanomaterials with desired properties.[35] For example, using BC as template, uniform spherical ZnO nanoparticles could be incorporated into BC fibers, and the resulted nanocomposites showed good mechanical properties and high photocatalytic activity.[36,37] Zheng *et al.*[38] synthesized ZnO nanoparticles by *in situ* polyol method with the freshly prepared water-wet amidoximated bacterial cellulose (Am-BC) serving as an effective nanoreactor, and found that the loading content of ZnO nanoparticles is higher using Am-BC as a template than using the unmodified BC. It was also reported that monolithic, lightweight and hierarchically porous zinc oxide bionanocomposite foams could be assembled through the mediation of bacterial cellulose, and the obtained zinc oxide/BC foam exhibit excellent antibacterial activity under both daylight and UV light.[39] Busuioc *et al.*[40] fabricated 3D calcium phosphate based scaffolds using BC as template which resemble the natural bone. However, although BC has many advantages as a template in synthesis of functional materials, preparation of urchin-like Cs_xWO_3 particles by hydrothermal reaction using BC as a template has not been reported.

Therefore, in this paper, urchin-like Cs_xWO_3 particles were first synthesized using BC as a template by hydrothermal method. After H_2 heat-treatment, the urchin-like particles could be transformed into small size nanorods with exhibiting excellent visible light transparency and thermal insulation performance. It has been confirmed that abnormal growth of Cs_xWO_3 rods was greatly reduced after introduction of BC into the precursor solution. Moreover, the small size of Cs_xWO_3 nanorods could significantly improve the transparent heat-insulation properties of Cs_xWO_3 film. The synthesized Cs_xWO_3 particles with small size are of great significance for realizing its practical applications in the field of energy-saving glasses. Meanwhile, this synthesis strategy can also be expected to be suitable for synthesizing other functional small size nanoparticles.

2. Experimental section

2.1. Preparation of Cs_xWO_3 powders

Cesium sulfate (Cs_2SO_4), sodium tungstate ($Na_2WO_4 \cdot 2H_2O$) and citric acid ($C_6H_8O_7 \cdot H_2O$) (CA) are all analytical reagents and used as raw materials. The bacterial cellulose (BC, ShangHai YiFang Rural Technology Holdings Co. Ltd) was heated to 90 °C in a concentrated 2 M KOH solution for 6 h, and the obtained darken BC was washed repeatedly with deionized water until it is translucent so as to remove sugar. And then, it was made into paste with a juicer.

Cs_xWO_3 powders were prepared by hydrothermal reaction and subsequent thermal reduction method using sodium tungstate as W source and cesium sulfate as Cs source, respectively. Firstly, sodium tungstate solution with concentration of 0.25 mol L^{-1} was ion exchanged with Amberlite (Strongly Acid Styrene Type Cation Exchange Resin) to obtain yellowish tungstic acid solution. Then, a certain amount of BC, citric acid, cesium sulfate and ionized water were sequentially added to 77 mL of the tungstic acid solution under stirring to obtain a precursor solution. The amount of citric acid and cesium sulfate added was 22.552 g and 1.742 g, respectively. The BC addition amount was 5 mL, 20 mL and 30 mL respectively and the total volume of the precursor solution was 110 mL. Then the precursor solution was transferred into a Teflon-lined autoclave with 200 mL internal volume, and hydrothermal reaction was conducted at 190 °C for 72 h. The obtained blue precipitates were then collected by centrifugation and washing with deionized water and ethanol three times respectively, and finally dried at 70 °C. The as-prepared Cs_xWO_3 samples with adding 0 mL, 5 mL, 20 mL and 30 mL in the precursor solution were named as 0BC-Cs_xWO_3, 5BC-Cs_xWO_3, 20BC-Cs_xWO_3 and 30BC-Cs_xWO_3, respectively. Finally, the dried products were heat-treated (HT) under H_2 atmosphere at 550 °C for 2 h and dark blue Cs_xWO_3 powders were obtained, which were named as 0BC-HT-Cs_xWO_3, 5BC-HT-Cs_xWO_3, 20BC-HT-Cs_xWO_3 and 30BC-HT-Cs_xWO_3, respectively. In addition, in order to investigate the formation mechanism of urchin-like Cs_xWO_3 particles, synthesis of Cs_xWO_3 by hydrothermal reaction for a shorter time (1.5–8 h) was also conducted. Each of our Cs_xWO_3 samples was synthesized more than 6 times, and the microscopic size of the prepared urchin-like Cs_xWO_3 crystals fluctuates by about ±10%. It has been found that the samples prepared by this method have excellent reproducibility.

2.2. Preparation of Cs_xWO_3 films

Cs_xWO_3 thin films were prepared from polyvinyl alcohol (PVA) dispersion of Cs_xWO_3 particles with PVA as film former. Firstly, Cs_xWO_3 powders were dispersed in 12 wt% PVA aqueous solution in 80 °C water bath so as to obtain the coating liquid with good dispersibility. Subsequently, Cs_xWO_3 thin films were uniformly coated on the surface of glass slides by roll coating method.

2.3. Characterization

The phase compositions of the Cs_xWO_3 particles were determined by X-ray diffraction analysis (XRD, D/max-3B, Japan) using graphite-monochromized Cu Kα radiation. The size and shape of the nanoparticles were observed by scanning electron microscopy (SEM, JEOL JSM-7800F, Japan) and transmission electron microscopy (TEM, JEOL JEM-2100 UHR). The Fourier transform infrared (FTIR) spectra were recorded on a Spectrum two in the wave number range of 450 and 4000 cm^{-1}. The surface composition of the sample and the binding energies of W in the sample were determined by X-ray photoelectron

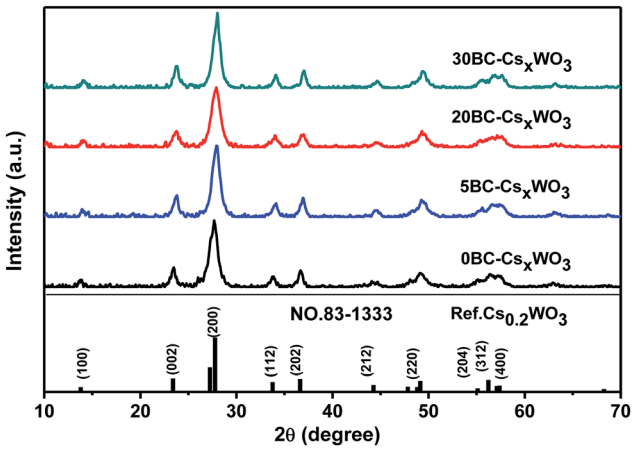

Fig. 1 XRD patterns of nBC-Cs$_x$WO$_3$ particles (n = 0; 5; 20; 30).

spectroscopy (XPS, ESCALAB 250). The UV-Vis-NIR transmittance spectra at wavelength 300–1100 nm and 300–2500 nm of the Cs$_x$WO$_3$ sample powders were measured using a modular solar cell spectral performance testing system (7-SCSpecIII–Beijing Saifan Photoelectric Instrument Co., Ltd.) and a UV-Vis-NIR spectrophotometer (Lambda 950, Perkin Elmer), respectively. Moreover, the thermal insulation performance of the glasses coated with Cs$_x$WO$_3$ film was evaluated by a simulated thermal insulation chamber with the top window glass being irradiated by a 250 W infrared lamp.

3. Results and discussion

3.1. Effects of the BC on the microstructure and properties

Fig. 1 shows the XRD patterns of Cs$_x$WO$_3$ particles synthesized by hydrothermal method with adding different amount of BC into the precursor solution. The XRD patterns of the obtained Cs$_x$WO$_3$ powders showed that the as-prepared Cs$_x$WO$_3$ products with different amount of BC all exhibited hexagonal tungsten bronze structure corresponding to the standard pattern of Cs$_{0.2}$WO$_3$ (JCPDS no. 83-1333). The average crystal size of nBC-Cs$_x$WO$_3$ was calculated by using the Scherrer formula. As is shown in Table 1, the average crystal size of 20BC-Cs$_x$WO$_3$ and 30BC-Cs$_x$WO$_3$ is less than 230 Å.

Fig. 2a–d shows the TEM images of nBC-Cs$_x$WO$_3$ particles synthesized by hydrothermal method with adding different amount of BC into the precursor solution. It can be seen that there were a large number of abnormally grown Cs$_x$WO$_3$ grains in the prepared particles when no BC was added in the precursor solution. By contrast, the TEM images of the as-prepared Cs$_x$WO$_3$ powders showed that most of the obtained Cs$_x$WO$_3$ particles were urchin-like when 5 mL BC were added into the precursor solution, and some abnormally grown individual nanorod-like particles could also be visible. Whereas, when 20 mL BC were added into the precursor solution, the synthesized Cs$_x$WO$_3$ particles almost all exhibited urchin-like with diameter of 100–300 nm, which indicated that the added BC could promote the nucleation and uniform growth of Cs$_x$WO$_3$ particles. The corresponding EDS element mapping in Fig. 2f–h display the elemental distribution of W, O, and Cs, indicating the successful growth of Cs$_x$WO$_3$ particles.

FTIR measurements were conducted to clarify whether BC is completely decomposed during solvothermal reaction. By comparing the FTIR spectra of the samples 0BC-Cs$_x$WO$_3$ and 20BC-Cs$_x$WO$_3$ in Fig. 3, it can be seen that the absorption peaks of the two samples are almost same and no typical absorption peaks of BC appeared. Especially, the absence of the C–O–C pyranose ring skeletal vibration[35] indicates that the BC was completely decomposed after solvothermal reaction.

Fig. 4a shows the formation mechanism of urchin-like Cs$_x$WO$_3$ particles under the induction of BC. Firstly, the filamentous structure of BC may be fast decomposed by citric acid and breaks off in the reaction system under high temperature and high pressure. The citric acid may be enriched on the surface of the broken BC owing to the esterification reaction in eqn (1). During the hydrothermal reaction, the main role of citric acid is to provide H^+ and create a reduction atmosphere. It is only in the reduction atmosphere that the rod-like Cs$_x$WO$_3$ particles with hexagonal structure can be formed. As is reported, citric acid has three carboxyl groups and one hydroxyl group. The β-carboxyl group is prone to decarboxylation to produce acetone dicarboxylate, carbon dioxide, hydrogen ions (H^+) and free hydrogen atom ([H]). The free [H] takes away oxygen atoms of [WO$_6$] octahedrons to produce oxygen vacancies while reducing W^{6+} to W^{5+} and promoting Cs^+ ions entering the hexagonal tunnels of tungsten bronze. It was proved that citric acid could promote the formation of W^{5+} and meanwhile urge Cs^+ to access the hexagonal tunnel of [WO$_6$].[31] Therefore, on the premise that citric acid provides reducing atmosphere, the Cs$_x$WO$_3$ nanorods will grow gradually on the debris of BC, and the broken BC will provide a sufficient physical interface for the nucleation of Cs$_x$WO$_3$ crystals. As a result, urchin-like Cs$_x$WO$_3$ particles were formed under the induction of BC.

Table 1 The average crystal size, XPS analysis results and transparent heat insulation properties of the as prepared nBC-Cs$_x$WO$_3$ powders

Sample	Average crystal size (Å)	Content ratio of W^{5+}/W^{6+}	T_{Vis}[a] (%)	T_{NIR}[b] (%)	THI[c]
0BC-Cs$_x$WO$_3$	834	0.1 : 1	44.8	31.9	1.4
5BC-Cs$_x$WO$_3$	405	—	55.2	30.1	1.83
20BC-Cs$_x$WO$_3$	223	0.08 : 1	60.6	29.6	2.05
30BC-Cs$_x$WO$_3$	207	—	56.7	29.2	1.94

[a] T_{Vis} means the maximum transmittance of visible light. [b] T_{NIR} means the transmittance at 1100 nm. [c] THI means the transparent heat insulation index: THI = T_{Vis}/T_{NIR}.

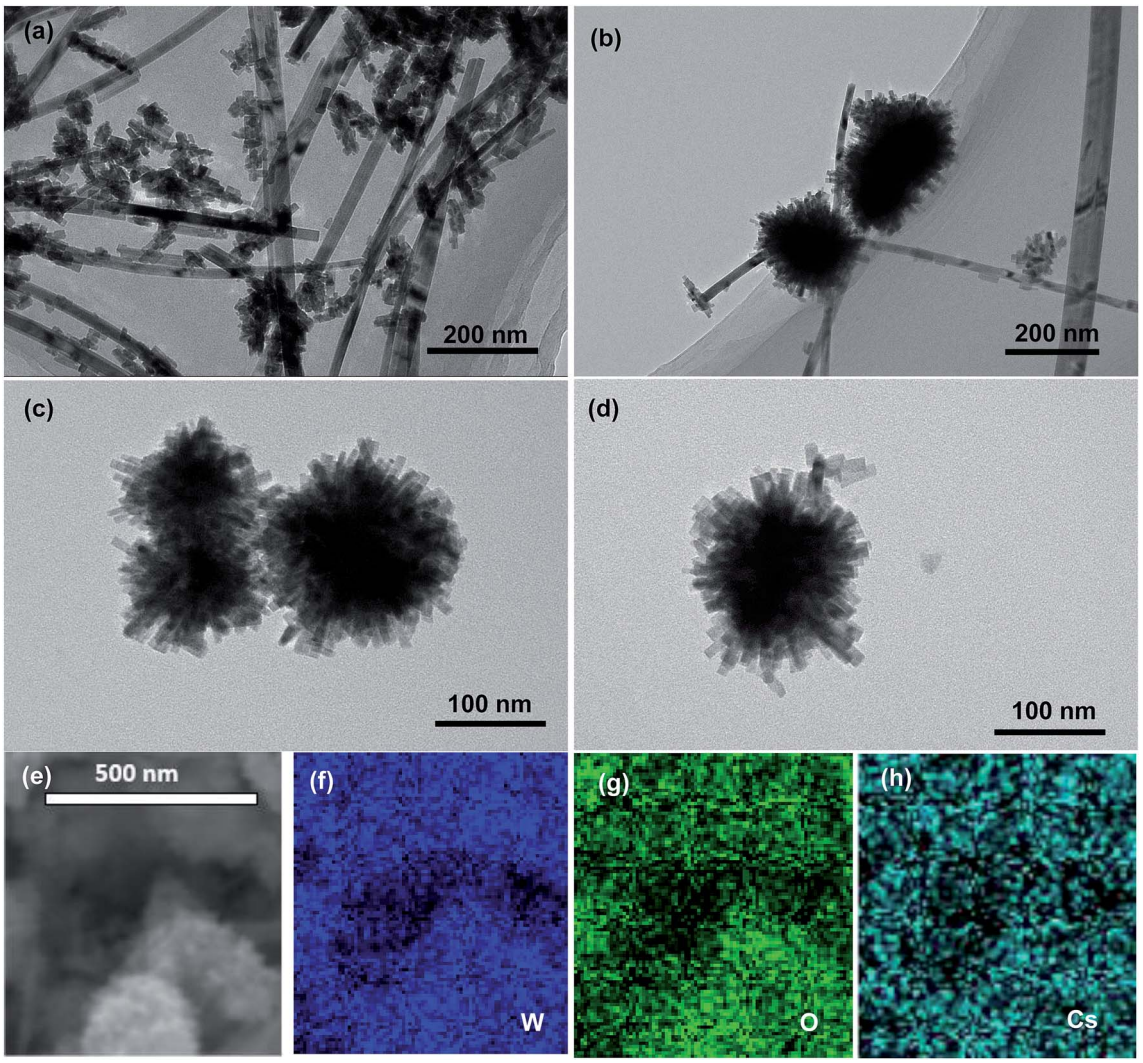

Fig. 2 TEM images of Cs_xWO_3 particles with different BC addition amount in the precursor solution (a) BC = 0 mL; (b) BC = 5 mL; (c) BC = 20 mL; (d) BC = 30 mL. (e) SEM images of 20BC-Cs_xWO_3 particles. The corresponding EDS elemental mappings of 20BC-Cs_xWO_3 particles: (f) W, (g) O, and (h) Cs.

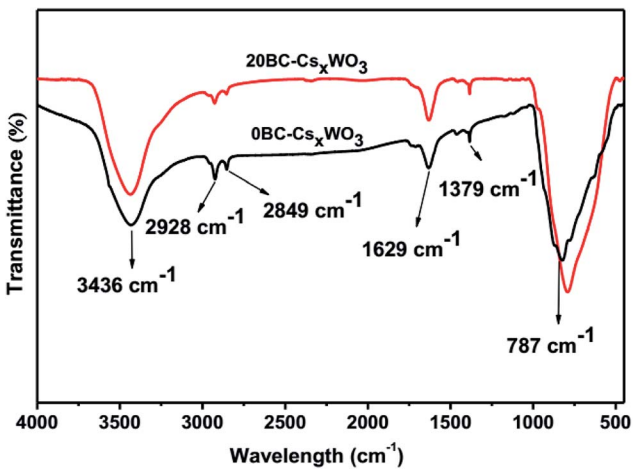

Fig. 3 The FTIR spectra of the samples 0BC-Cs_xWO_3 and 20BC-Cs_xWO_3.

Fig. 4b shows the SEM image of BC sample obtained by freeze drying. It is found that the average diameter of BC is about 50 nm. The minor-diameter BC is prone to breakage during hydrothermal reaction under high temperature and pressure, which induced the formation of urchin-like Cs_xWO_3 particles.

Fig. 4c illustrates the schematic diagram of the hexagonal structure of Cs_xWO_3 crystal projected on *a*–*b* plane, where the angle between the *a*-axis and *b*-axis is 120°. During the crystal growth process, the Cs_xWO_3 particles can grow along the direction parallel to *c*-axis or perpendicular to the *c*-axis.[28] The $[WO_6]$ octahedron reacts with each other by the oxygen at its apex combining with [H], then the two $[WO_6]$ octahedrons are successfully connected with the bridge oxygen and meanwhile one water is released. At the same time, the reductive [H] produced from citric acid will reduce part of W^{6+} to W^{5+}, and these W^{5+} can attract Cs^+ into the hexagonal tunnel formed by $[WO_6]$ octahedrons under the action of electric field force.[1]

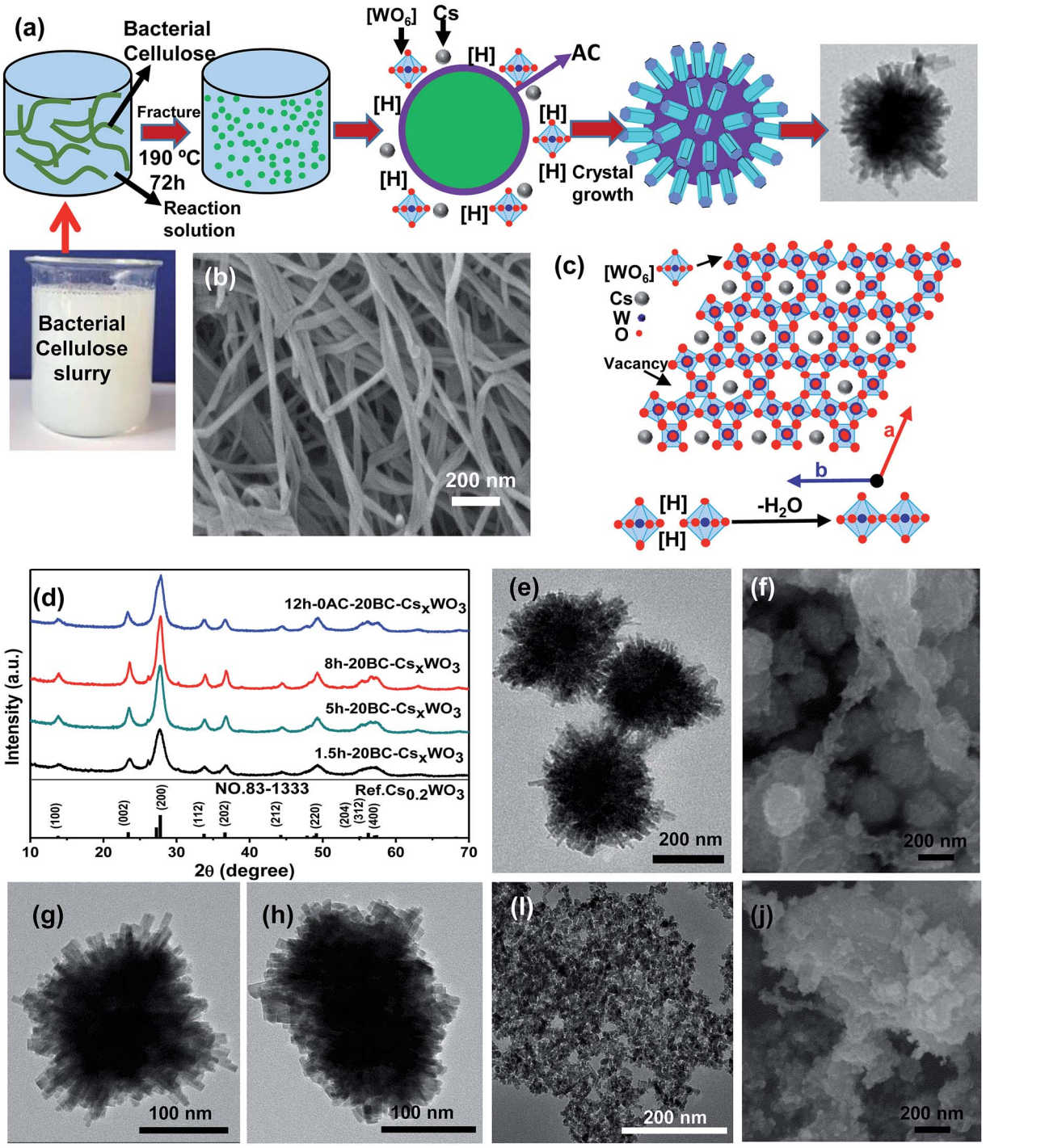

Fig. 4 (a) The formation mechanism diagram of urchin-like Cs_xWO_3 particles using BC as template; (b) SEM image of BC obtained by freeze drying; (c) the schematic diagram of Cs_xWO_3 crystal structure and the reaction between $[WO_6]$ octahedrons; (d) XRD patterns: 20BC-Cs_xWO_3 powders synthesized by hydrothermal synthesis for 1.5 h, 5 h, 8 h and 20BC-Cs_xWO_3 powders synthesized by hydrothermal synthesis for 12 h without citric acid; (e) and (f) are the TEM and SEM image of the 20BC-Cs_xWO_3 powders synthesized by hydrothermal synthesis for 1.5 h, respectively; (g) and (h) are the TEM of the 20BC-Cs_xWO_3 powders synthesized by hydrothermal synthesis for 5 h and 8 h, respectively; (i) and (j) are the TEM and SEM image of the 20BC-Cs_xWO_3 powders synthesized by hydrothermal synthesis for 12 h without citric acid, respectively.

However, it can be seen from Fig. 1 that the synthesized Cs_xWO_3 particles exhibit $Cs_{0.2}WO_3$ structure. The doping amount of Cs element is lower than the saturation value (Cs : W = 0.33 : 1),[28] which may be due to the lower W^{5+} amount in the products, and thus part of the hexagonal tunnel is not filled with Cs^+.

Fig. 4d shows the XRD patterns of 20BC-Cs_xWO_3 powders synthesized by hydrothermal synthesis for 1.5 h, 5 h and 8 h. The XRD patterns of the obtained Cs_xWO_3 powders showed that the as-prepared Cs_xWO_3 products with different reaction time all exhibited hexagonal tungsten bronze structure

corresponding to the standard pattern of $Cs_{0.2}WO_3$ (JCPDS no. 83-1333). In addition, it can be clearly seen that the diffraction peak of the crystal increases obviously with the increase of reaction time, which means that the crystallinity is further improved. From the XRD patterns of 20BC-Cs_xWO_3 powders synthesized by hydrothermal synthesis for 12 h without citric acid, it can be seen that the product also exists in the form of $Cs_{0.2}WO_3$ crystals.

Fig. 4e and f are the TEM and SEM images of the 20BC-Cs_xWO_3 powders synthesized by hydrothermal synthesis for 1.5 h, respectively. It can be seen that a large number of urchin-like Cs_xWO_3 particles with a diameter of about 200 nm are synthesized in only 1.5 h of hydrothermal reaction time. As shown in Fig. 4f, a small amount of fiber structure can still be found with the length being about 500 nm. Fig. 4g and h are the TEM images of the 20BC-Cs_xWO_3 powders synthesized by hydrothermal synthesis for 5 h and 8 h, respectively. It can be seen that the urchin-like Cs_xWO_3 has no obvious change in morphology with the extension of the reaction time. Fig. 4i and j are the TEM and SEM images of the 20BC-Cs_xWO_3 powders synthesized by hydrothermal synthesis for 12 h without citric acid, respectively. It can be seen that the as-prepared samples without citric acid are small dispersive crystal grains, and no urchin-like particles are found. By comparison with Fig. 2a, it can be seen that the addition of BC can significantly inhibit the abnormal growth of crystal grains, resulting in a decrease in the grain size and an increase in the uniformity, but only BC can not promote the formation of urchin-like morphology. Furthermore, citric acid plays an important role in the synthesis of urchin-like Cs_xWO_3, which may be related to the enrichment of citric acid on the surface of BC fragments.

reaction system is complicated because of the breakage and decomposition of BC, thus it is difficult to characterize accurately the esterification reaction products. However, it has been clarified that the product 30BC-Cs_xWO_3 with 30 mL BC addition in the precursor solution exhibited lower NIR shielding ability than the sample 20BC-Cs_xWO_3 owing to the excess esterification, as is shown in Fig. 5.

The UV-Vis-NIR transmission spectra of glasses coated with Cs_xWO_3 films with different amount of BC in the precursor solution are shown in Fig. 5a. It is observed that the addition amount of BC has a great influence on the transmittance spectra of the products. In order to characterize the performance of different films, three characterization parameters, namely maximum transmittance of visible light (T_{Vis}), transmittance at 1100 nm (T_{NIR}) and transparent heat insulation index (THI), are introduced, and the obtained corresponding values of different films are listed in Table 1. The larger the T_{Vis} and THI of films, the better the transparent heat insulation performance of films. As for the Cs_xWO_3 sample prepared without BC, the visible transparency is poor with the maximum transmittance of visible light (T_{Vis}) being only 44.8% which is because that the larger grain size hinders the transmittance of visible light. Whereas, the Cs_xWO_3 sample prepared with using BC as template showed obvious improved visible transmittance. Moreover, with the increase of BC addition amount, the visible light transmittance of the samples increases obviously due to the decrease of the grain size. Especially, the Cs_xWO_3 sample prepared with adding 20 mL BC into the precursor solution exhibits highest visible light transmittance ($T_{Vis} = 60.6\%$) and better transparent heat insulation index (THI = 2.05) simultaneously. However, it is

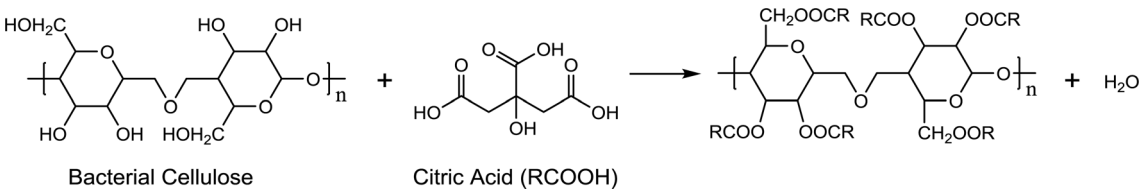

(1)

In addition, during the hydrothermal synthesis of Cs_xWO_3 products, the esterification reaction between the hydroxyl group (–OH) in BC and the carboxyl group (–COOH) in citric acid (RCOOH) occurs to some extent, as is shown in eqn (1). It is reasonable to infer that the reducing atmosphere in the reaction solution may be changed or decreased because the esterification reaction will consume some citric acid. Especially, when excess BC is added in the precursor solution, the reducibility of the reaction system will be greatly reduced owing to the high consumption of citric acid, which is not conducive to Cs^+ entering the hexagonal tunnels and formation of hexagonal Cs_xWO_3 crystals. Of course, the esterification reaction between BC and citric acid occurring in the hydrothermal

noteworthy that when the amount of BC added is 30 mL, the visible light transmittance decreases again ($T_{Vis} = 56.7\%$). This may be due to the decrease of the reducibility in the reaction system owing to the reaction between hydroxyl groups (–OH) in the bacterial cellulose and carboxyl groups (–COOH) in the citric acid (see eqn (1)). According to our previous research work,[30] the maximum visible light transmittance of the Cs_xWO_3 powder synthesized by hydrothermal method is about 63%, and the transmittance at 1100 nm is about 50%. It can be seen from the comparison that the Cs_xWO_3 products prepared with the induction of BC in this work has better NIR shielding properties than that without BC in the precursor solution.

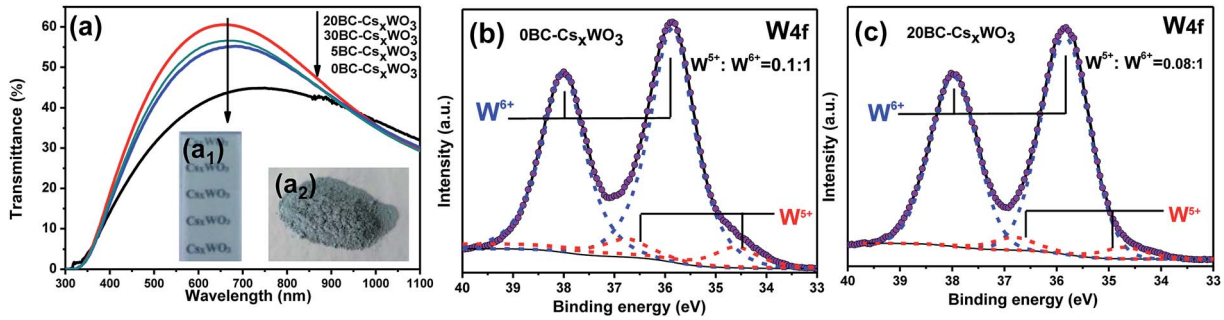

Fig. 5 (a) The UV-Vis-NIR transmittance spectra of nBC-Cs$_x$WO$_3$ films (the inset (a$_1$) and (a$_2$) are photographs of the 20BC-Cs$_x$WO$_3$ film and powders, respectively); (b) W$_{4f}$ core-level XPS spectra of 0BC-Cs$_x$WO$_3$; (c) W$_{4f}$ core-level XPS spectra of 20BC-Cs$_x$WO$_3$.

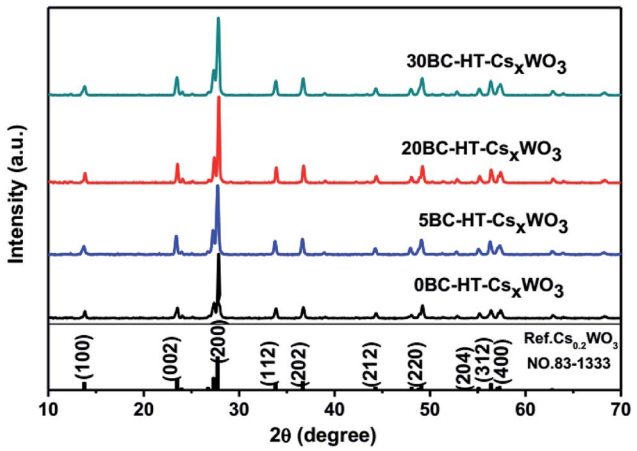

Fig. 6 XRD patterns of nBC-HT-Cs$_x$WO$_3$ particles (n = 0; 5; 20; 30).

Fig. 5b and c show the W$_{4f}$ XPS spectra of samples 0BC-Cs$_x$WO$_3$ and 20BC-Cs$_x$WO$_3$, respectively. The deconvolution of W$_{4f}$ core-level spectrum can be fitted into two doublets, associated with two different valence states of W atoms. The first doublet, having a W$_{4f}^{5/2}$ at 37.9 eV and a W$_{4f}^{7/2}$ at 35.9 eV, may be attributed to the W^{6+}. The second doublet, with relative lower binding energy at 34.5 eV and 36.7 eV, may be resulted from the emission of W$_{4f}^{5/2}$ and W$_{4f}^{7/2}$ core levels corresponding to W^{5+}.[25] It can be seen that the W^{5+}/W^{6+} ratio in 20BC-Cs$_x$WO$_3$ sample (W^{5+}/W^{6+} = 0.08) is slightly lower than that of 0BC-Cs$_x$WO$_3$ without BC (W^{5+}/W^{6+} = 0.1), which is related to the esterification reaction as is shown in eqn (1). It can be concluded that appropriate BC addition amount is favorable for improving the visible transparency and near-infrared shielding ability of Cs$_x$WO$_3$ products.

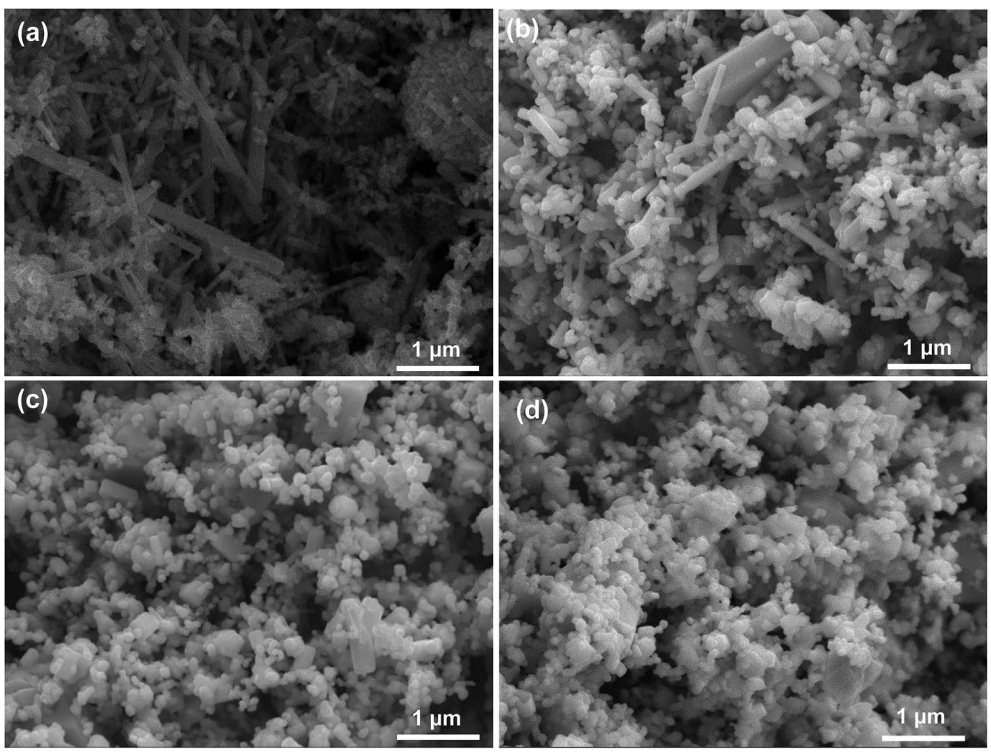

Fig. 7 SEM images of Cs$_x$WO$_3$ products synthesized with adding different amount of BC as template after H$_2$ heat-treatment: (a) BC = 0 mL; (b) BC = 5 mL; (c) BC = 20 mL; (d) BC = 30 mL.

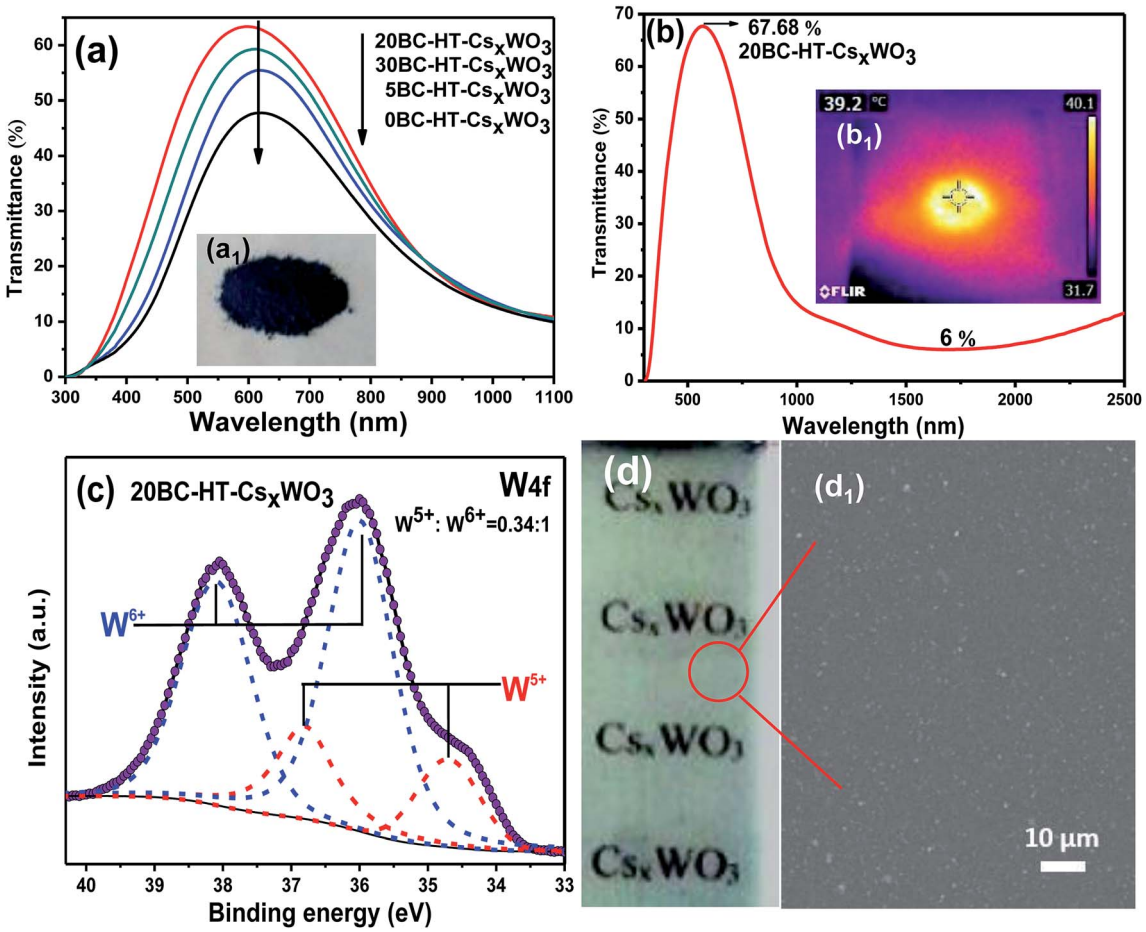

Fig. 8 (a) The UV-Vis-NIR transmittance spectra (300–1100 nm) of *n*BC-HT-Cs_xWO_3 films with different BC addition amount (the inset photographs (a_1) is the Cs_xWO_3 powders); (b) the UV-Vis-NIR transmittance spectra (300–2500 nm) of 20BC-HT-Cs_xWO_3 film (the inset photograph (b_1) is the thermographic image of 20BC-HT-Cs_xWO_3 powders irradiated by a 250 W infrared lamp for 0.5 min); (c) XPS spectra of the 20BC-HT-Cs_xWO_3 samples: deconvolution of W_{4f} core-level spectrum with peaks corresponding to W^{6+} and W^{5+}; (d) the glass coated with 20BC-HT-Cs_xWO_3 film and (d_1) is SEM images of 20BC-HT-Cs_xWO_3 film.

3.2. Effects of hydrogen heat treatment

Fig. 6 shows the XRD patterns of Cs_xWO_3 particles with different BC addition amount after H_2 heat-treatment at 550 °C for 2 h. It can be seen that the Cs_xWO_3 powders still exist in the form of hexagonal $Cs_{0.2}WO_3$ crystals and the crystallinity of the particles could be further increased after H_2 heat-treatment.

Fig. 7 shows the SEM images of Cs_xWO_3 particles synthesized with adding different amount of BC as template after H_2 heat-treatment. As for the Cs_xWO_3 particles without BC in the precursor solution, the grain size is generally large, and there are a great number of rod-like crystals with length more than 1 μm, which is not favorable for attaining to higher transparent thermal insulation performance of Cs_xWO_3 films. Whereas, after H_2 heat-treatment, the morphology of Cs_xWO_3 samples with using BC as template changed from the original urchin-like particles (as is shown in Fig. 2b–d) into smaller individual grains (see Fig. 7b and c). Moreover, with the increase of BC in the precursor solution, the uniformity of Cs_xWO_3 particles increase and the grain size of Cs_xWO_3 particles tend to become smaller. Particularly, the urchin-like morphology of 20BC-HT-Cs_xWO_3 and 30BC-HT-Cs_xWO_3 samples almost completely disappeared, changing into individual particles with size less than 1 μm and the particle size being mainly between 100–200 nm (see Fig. 7c and d). The small and uniform particle size is advantageous for the uniform dispersion of Cs_xWO_3 particles in the film, which is favorable for increasing the visible light transmittance of the Cs_xWO_3 films.

The UV-Vis-NIR transmission spectra of glasses coated with different Cs_xWO_3 films after heat-treatment are shown in Fig. 8a and b. It is observed that the 0BC-HT-Cs_xWO_3 film without adding BC in the precursor solution has lower visible light transmittance with the maximum visible light transmittance being only 47.7%. Whereas, the 20BC-HT-Cs_xWO_3 film exhibits the highest visible light transmittance with the maximum visible light transmittance (T_{vis}) being 63.4% and transparent heat insulation index (THI) being 5.84. The maximum visible light transmittance of 30BC-HT-Cs_xWO_3 film is 59.2%, which is slightly lower than that of 20BC-HT-Cs_xWO_3. In addition, it can also be seen from Fig. 8b that the 20BC-HT-Cs_xWO_3 sample has excellent near-infrared shielding performance in the

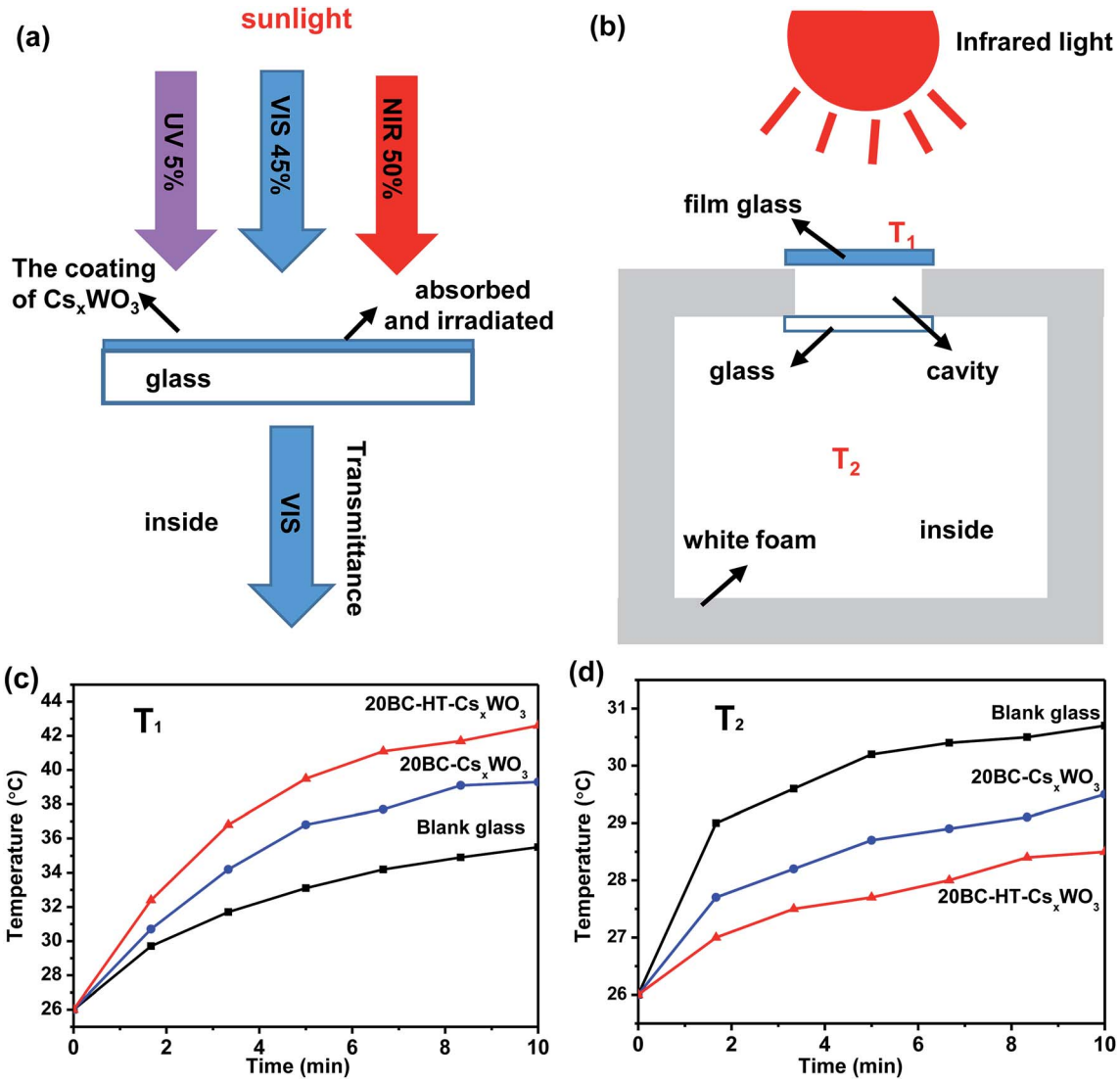

Fig. 9 (a) Schematic diagram of transparent thermal insulation mechanism of glass coated with Cs_xWO_3 film; (b) schematic diagram of cross-section of the thermal insulation performance test device; (c) the surface temperature T_1 of the blank glass or Cs_xWO_3 film glass varying curves with infrared lamp irradiation time; (d) the inside temperature T_2 of the polystyrene box varying curves with infrared lamp irradiation time.

wavelength range of 1100–2500 nm and the minimum near-infrared transmittance is only 6%. According to our previous research work,[31] the maximum visible light transmittance of the heat treated Cs_xWO_3 powder synthesized by solvothermal method is about 77–78%, and the transmittance at 2500 nm is more than 20%. Fig. $8d_1$ shows the SEM images of 20BC-HT-$Cs_{xg}WO_3$ film. It can be found that the Cs_xWO_3 particles are uniformly dispersed in the PVA film.

In addition, the film has a UV blocking rate of more than 80% at wavelength of 360 nm and an apparent tendency to increase the blocking rate of UV with decreasing wavelength. As is shown in Fig. $8b_1$, the surface temperature of the powder increased rapidly from 12 °C to 39.2 °C after exposed to infrared light for 0.5 min, showing a good infrared absorption ability. By comprehensive analysis of Fig. 5a and Fig. 8a and b, it can be concluded that H_2 heat-treatment can further promote the transparent heat-insulation performance of the Cs_xWO_3 powders and the sample 20BC-HT-Cs_xWO_3 exhibits the best visible light transmittance.

As is shown in Fig. 8c, there is also a certain amount of W^{5+} in the sample 20BC-HT-Cs_xWO_3 apart from the W^{6+}, and the W^{5+}/W^{6+} ratio is 0.34 : 1, which is much bigger than that of the sample before H_2 heat-treatment. After H_2 heat-treatment, the chemical formula of Cs_xWO_3 particles can be expressed as $Cs_xW_x^{5+}W_{1-x}^{6+}O_3$. The improvement of the visible light transmittance and near-infrared shielding ability of Cs_xWO_3 products can be mainly attributed to the increase of W^{5+} content in Cs_xWO_3 particles.

In this experiment, the thermal-insulation performance of the Cs_xWO_3 film was tested using an infrared lamp of 250 W as a heat source. Fig. 9a shows the transparent thermal-insulation mechanism of Cs_xWO_3 films, which can absorb most of the infrared light while allowing most visible light to pass through.

Fig. 9b shows the schematic diagram of the cross-section of the device for testing thermal-insulation properties, where T_1 is the surface temperature of the Cs_xWO_3 film and T_2 is the air temperature in the foam box. Fig. 9c and d show the curves of the temperatures T_1 and T_2 with the increase of the irradiation time for blank glass and different Cs_xWO_3 film glass samples, respectively.

The temperature curve of Fig. 9c shows that the surface temperature T_1 of the 20BC-HT-Cs_xWO_3 sample increases most rapidly with the irradiation time of infrared lamp. The surface temperature T_1 of the film reached 42.6 °C within 10 min of infrared light irradiation, indicating that it has good infrared absorption ability. In addition, the surface temperature of the 20BC-Cs_xWO_3 films was between that of the blank glass and the 20BC-HT-Cs_xWO_3 films.

Fig. 9d shows the inside air temperature T_2 of the polystyrene box varying curves with infrared lamp irradiation time. It can be observed that the inside air temperature of the box corresponding to the blank glass attains to 30.7 °C with an increase of 4.7 °C from the room temperature (26 °C). Whereas, the inside air temperature corresponding to 20BC-Cs_xWO_3 film sample has a lower increase of 1.2 °C than that of the blank glass. Moreover, the 20BC-HT-Cs_xWO_3 film exhibits the best thermal insulation performance, and the inside air temperature T_2 only attains to 28.5 °C with increasing by only 2.5 °C from the room temperature after infrared lamp irradiation for 10 min. This result indicates that the 20BC-HT-Cs_xWO_3 film has excellent thermal insulation performance, which is especially appropriate for applications of energy-saving window glasses in the tropical region, so as to improve the human body comfort and reduce emissions caused by air-conditioning.

4. Conclusion

The urchin-like Cs_xWO_3 particles were synthesized by hydrothermal reaction using sodium tungstate as W source and bacterial cellulose (BC) as template. It has been proved that the introduction of BC template can significantly inhibit the abnormal growth of Cs_xWO_3 nanorods, and is favorable for obtaining urchin-like particles with uniform distribution and small size. Compared with Cs_xWO_3 synthesized without BC, the as-prepared Cs_xWO_3 products using BC template had apparent improved visible light transparency. Especially the 20BC-Cs_xWO_3 sample with appropriate BC amount exhibited better visible light transmittance, with the visible light transmittance (T_{Vis}) being more than 60%. After H_2 heat-treatment, the urchin-like particles were transformed into nanorods with excellent visible transparency and thermal insulation performance. In particular, it has been proved that the 20BC-HT-Cs_xWO_3 film has excellent thermal insulation performance, and has broad application prospects in the field of solar heat filter and energy-saving window glasses.

Conflicts of interest

There are no conflicts to declare.

Acknowledgements

This work was financially supported by the National Natural Science Foundation of China (No. 51278074, 51778098), the 2015 Science & Technology Project by the Ministry of Housing and Urban-Rural Development of China (2015-K1-042), the 2016 Dalian City Construction Science & Technology Project (201612), the 2015 Liaoning Province Colleges and Universities Outstanding Talent Support Program (LR2015005) and Dalian Science & Technology Innovation Fund (2018J12SN066).

References

1 S. Ran, J. X. Liu, F. Shi, C. Y. Fan, B. Chen, H. M. Zhang, L. Yu and S. H. Liu, *Sol. Energy Mater. Sol. Cells*, 2018, **174**, 342–350.
2 J. X. Liu, C. Y. Fan, F. Shi, L. Yu, X. Huang, S. C. Hu, B. Chen, S. Ran and S. H. Liu, *Mater. Lett.*, 2016, **181**, 140–143.
3 J. X. Liu, Q. Xu, F. Shi, S. H. Liu, J. Y. Luo, L. Bao and X. Feng, *Appl. Surf. Sci.*, 2014, **309**, 175–180.
4 H. T. Liu, X. F. Zeng, X. R. Kong, S. G. Bian and J. F. Chen, *Appl. Surf. Sci.*, 2012, **22**, 8564–8569.
5 P. Tao, A. Viswanath, L. S. Schadler, B. C. Benicewicz and R. W. Siegel, *ACS Appl. Mater. Interfaces*, 2011, **3**, 3638–3645.
6 J. Qu, J. R. Song, J. Qin, Z. N. Song, W. D. Zhang, Y. X. Shi, T. Zhang, H. Q. Zhang, R. P. Zhang, Z. Y. He and X. Xue, *Energy Build.*, 2014, **77**, 1–10.
7 S. D. Ji, F. Zhang and P. Jin, *Sol. Energy Mater. Sol. Cells*, 2011, **95**, 3520–3526.
8 C. S. Guo, S. Yin, M. Yan, M. Kobayashi, M. Kakihana and T. Sato, *Inorg. Chem.*, 2012, **51**, 4763–4771.
9 H. Takeda and K. Adachi, *J. Am. Ceram. Soc.*, 2007, **12**, 4059–4061.
10 C. S. Guo, S. Yin, L. J. Huang and T. Sato, *ACS Appl. Mater. Interfaces*, 2011, **3**, 2794–2799.
11 Z. J. Gu, Y. Ma, T. Y. Zhai, B. F. Gao, W. S. Yang and J. N. Yao, *Chem. Eur. J.*, 2006, **12**, 7717–7723.
12 G. X. Liu, S. N. Wang, Y. T. Nie, X. H. Sun, Y. H. Zhang and Y. Tang, *J. Mater. Chem. A*, 2013, **1**, 10120–10129.
13 C. S. Guo, S. Yin, Q. Dong and T. Sato, *CrystEngComm*, 2012, **14**, 7727–7732.
14 C. S. Guo, S. Yin, Q. Dong, Y. F. Huang, H. H. Li and T. Sato, *Int. J. Nanotechnol.*, 2013, **10**, 126–133.
15 C. S. Guo, S. Yin, L. J. Huang, L. Yang and T. Sato, *Chem. Commun.*, 2011, **47**, 8853–8855.
16 Z. Y. Yu, Y. J. Yao, J. N. Yao, L. M. Zhang, Z. Chen, Y. F. Gao and H. J. Luo, *J. Mater. Chem. A*, 2017, **13**, 1–6.
17 J. X. Liu, F. Shi, X. L. Dong, S. H. Liu, C. Y. Fan, S. Yin and T. Sato, *Powder Technol.*, 2015, **270**, 329–336.
18 J. X. Liu, Y. Ando, X. L. Dong, F. Shi, S. Yin, K. Adachi, T. Chonan, A. Tanaka and T. Sato, *J. Solid State Chem.*, 2010, **183**, 2456–2460.
19 Y. Liu, L. Zhao, J. Z. Su, M. T. Li and L. J. Guo, *ACS Appl. Mater. Interfaces*, 2015, **7**, 3532–3538.
20 C. S. Guo, S. Yin, Q. Dong and T. Sato, *Nanoscale*, 2012, **4**, 3394–3398.

21 M. Yan, H. X. Gu, Z. Z. Liu, C. S. Guo and S. Q. Liu, *RSC Adv.*, 2015, **5**, 967–973.
22 C. S. Guo, H. J. Yu, B. Feng, W. D. Gao, M. Yan, Z. W. Zhang, Y. P. Li and S. Q. Liu, *Biomaterials*, 2015, **52**, 407–416.
23 W. J. Xu, Z. Q. Meng, N. Yu, Z. G. Chen, B. Sun, X. Z. Jiang and M. F. Zhu, *Nanoscale*, 2013, **5**, 6469–6478.
24 W. Guo, C. S. Guo, N. N. Zheng, T. D. Sun and S. Q. Liu, *Adv. Mater.*, 2017, **4**, 1–16.
25 W. J. Xu, Z. Q. Meng, N. Yu, Z. G. Chen, B. Sun, X. Z. Jiang and M. F. Zhu, *RSC Adv.*, 2015, **5**, 7074–7082.
26 G. L. Li, C. S. Guo, M. Yan and S. Q. Liu, *Appl. Catal., B*, 2016, **183**, 142–148.
27 X. Y. Wu, S. Yin, D. F. Xue, S. Komarnenic and T. Sato, *Nanoscale*, 2015, **7**, 17048–17054.
28 C. S. Guo, S. Yin, M. Yan and T. Sato, *J. Mater. Chem. A*, 2011, **21**, 5099–5105.
29 T. Y. Wang, Y. Li, J. P. Li, Z. H. Feng, D. F. Sun, B. Zhao, Y. H. Xu, R. X. Li and H. N. Cai, *RSC Adv.*, 2014, **4**, 43366–43370.
30 J. X. Liu, J. Y. Luo, F. Shi, S. H. Liu, C. Y. Fan, Q. Xu and G. L. Shao, *J. Solid State Chem.*, 2015, **221**, 255–262.
31 J. X. Liu, B. Chen, C. Y. Fan, F. Shi, S. Ran, J. Y. Yang, X. Song and S. H. Liu, *CrystEngComm*, 2018, **20**, 1509–1519.
32 Y. Q. Li, S. Y. Fu, Y. Yang and Y. W. Mai, *Chem. Mater.*, 2008, **20**, 2637–2643.
33 L. T. Kang, W. A. Xu, K. Wang, W. Liang, X. G. Liu, F. Gao, A. D. Lan, Y. Z. Yang and Y. F. Gao, *Sol. Energy Mater. Sol. Cells*, 2014, **128**, 184–189.
34 C. S. Guo, S. Yin, P. L. Zhang, M. Yan, K. Adachi, T. Chonanc and T. Sato, *J. Mater. Chem.*, 2010, **20**, 8227–8229.
35 J. M. Rajwade, K. M. Paknikar and J. V. Kumbhar, *Appl. Microbiol. Biotechnol.*, 2015, **99**, 2491–2511.
36 S. Chen, B. Zhou, W. Hu, W. Zhang, N. Yin and H. Wang, *Carbohydr. Polym.*, 2013, **92**, 1953–1959.
37 W. L. Hu, S. Y. Chen, B. H. Zhou and H. P. Wang, *Mater. Sci. Eng., B*, 2010, **170**, 88–92.
38 W. L. Zheng, W. L. Hu, S. Y. Chen, Y. Zheng, B. H. Zhou and H. P. Wang, *Chin. J. Polym. Sci.*, 2016, **32**, 169–176.
39 P. P. Wang, J. Zhao, R. F. Xuan, Y. Wang, C. Zou, Z. Q. Zhang, Y. Z. Wan and Y. Xu, *J. R. Soc. Med.*, 2014, **43**, 6762–6768.
40 C. Busuioc, M. Stroescu, A. Stoica-Guzun, G. Voicu and S. I. Jinga, *Ceram. Int.*, 2016, **14**, 15449–15458.